

# Topological multiferroic order in twisted transition metal dichalcogenide bilayers

Mikael Haavisto,<sup>1</sup> J. L. Lado,<sup>1</sup> and Adolfo O. Fumega<sup>1</sup>

<sup>1</sup>*Department of Applied Physics, Aalto University, 02150 Espoo, Finland*

Layered van der Waals materials have risen as powerful platforms to artificially engineer correlated states of matter. Here we show the emergence of a multiferroic order in a twisted dichalcogenide bilayer superlattice at quarter-filling. We show that the competition between Coulomb interactions leads to the simultaneous emergence of ferrimagnetic and ferroelectric orders. We derive the magnetoelectric coupling for this system, which leads to a direct strong coupling between the charge and spin orders. We show that, due to intrinsic spin-orbit coupling effects, the electronic structure shows a non-zero Chern number, thus displaying a topological multiferroic order. We show that this topological state gives rise to interface modes at the different magnetic and ferroelectric domains of the multiferroic. We demonstrate that these topological modes can be tuned with external electric fields as well as triggered by supermoire effects generated by a substrate. Our results put forward twisted van der Waals materials as a potential platform to explore multiferroic symmetry breaking orders and, ultimately, controllable topological excitations in magnetoelectric domains.

## INTRODUCTION

Twistronics has provided a new strategy to engineer correlated states stemming from the emergence of nearly flat moire bands[1–6]. Twisted bilayer graphene represents an early example of this, displaying nearly flat bands close to 1° rotation that become strongly correlated[1–4]. Twisted graphene multilayers provide thus a correlated model with strong interactions that can be easily controlled via electronic gating, leading to both symmetry broken[7–11] and topological states[12–14]. Other layered van der Waals materials including transition metal dichalcogenides (TMDs) represent an excellent building block to engineer a twisted system[15–23]. Specifically, TMDs monolayers can already display ordered phases[24, 25] that can be combined to form a twisted system. Moreover, they provide a source for spin-orbit coupling interactions[26–28], which may drive a non-trivial topological character in a the moire system[16]. Experimental realizations of twisted transition metal dichalcogenide heterostructures have shown emergent magnetic and charge order[15–23], including the emergence of strong magnetoelectric response[29]. However, the potential emergence of multiferroic order in an artificial twisted system remains relatively unexplored.

Multiferroic materials are characterized by the simultaneous existence of more than one symmetry breaking[30–32]. These multiple symmetry breaking materials display a strong coupling between their different order parameters. For the particular case of electric and magnetic orders, a magnetoelectric coupling[33] provides a venue for the electric control of magnetic orders, a feature with a huge potential interest. Different multiferroic mechanisms have been studied over the past years, both in bulk compounds[34–36] and recently in two-dimensional monolayers[37–39]. In the realm of moire materials, the strongly correlated states emerging in twisted systems provide an additional platform to artificially engineer

multiferroics associated with the moire length scale.

In this work, we show how a topological multiferroic order can be engineered in a twisted dichalcogenide bilayer. We start showing how twisted transition metal dichalcogenide homobilayers realize an effective correlated model in a staggered honeycomb superlattice. We show how the existence of competing long-range electronic interactions leads to the simultaneous emergence of ferrimagnetic and ferroelectric orders at quarter-filling. This multiferroic behavior is accompanied by a strong magnetoelectric coupling. Subsequently, we will analyze the necessary ingredients to turn this twisted multiferroic into a topological multiferroic. Finally, we show how the different ferroic domain walls that one can engineer in this topological system allow the magnetoelectric creation and control of topological Jackiw-Rebbi solitons. Our results put forward a strategy to obtain a multiferroic order in a twisted van der Waals heterostructure, and to exploit magnetoelectric control of multiferroic domains to engineer topological excitations.

## MODEL

We start by describing the heterostructure, consisting of two layers of a transition metal dichalcogenide twisted forming a moire pattern. The structure of the twisted TMD bilayer is shown in Fig. 1a, where each site corresponds to a transition metal atom. Two different inequivalent sites emerge: i) AA sites (yellow circles) where the transition metal atoms are perfectly aligned forming a triangular lattice and ii) two equivalent AB and BA sites (red circles) where the transition metal atoms are perfectly misaligned and form a staggered honeycomb lattice [40]. First principles and multiorbital Slater-Koster calculations[41–45] have shown the emergence of nearly flat bands in this twisted structure, stemming from the spatial modulation in the moire unit cell. The emergent moire mini bands feature localized states both in trian-

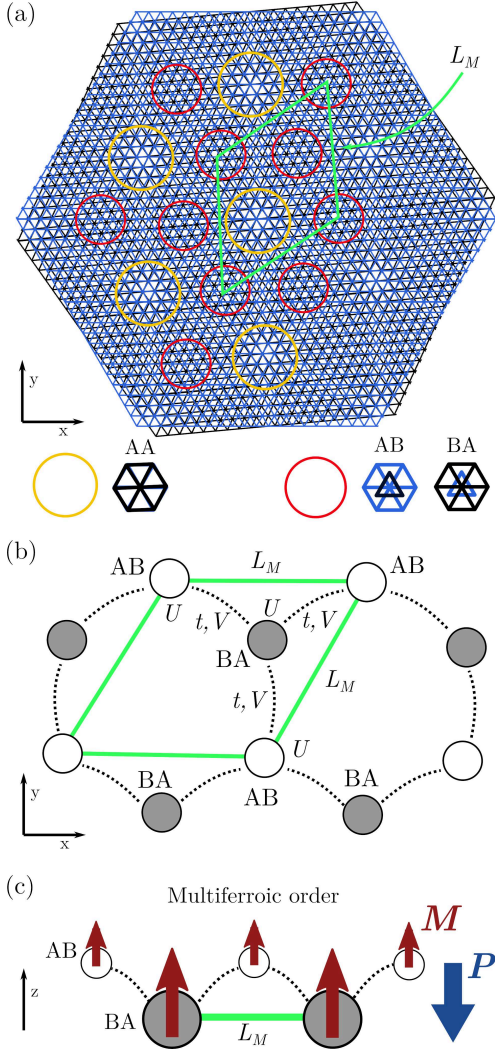


FIG. 1. (a) Schematic of the twisted bilayer triangular lattice associated with the transition metal  $M$  of the  $MX_2$ . Sites AB and BA are structurally equivalent and display a staggered honeycomb lattice with a lattice parameter corresponding to the moiré length  $L_M$ . (b) Staggered honeycomb lattice model. Moiré unit cell in green and AB (BA) sites are depicted as white (gray) circles. First neighbor hopping  $t$ , on-site  $U$ , and first neighbor  $V$  Coulomb interactions are schematically shown. (c) Emergent ferrimagnetic and fully gapped charge density wave orders from the quarter-filling staggered honeycomb model. In this state, the electric charge gets more localized in the BA sites which leads to an emergent electric polarization in the staggered honeycomb lattice.

gular and honeycomb lattices, corresponding to Wannier orbitals localized in the different stacking regions shown in Fig. 1a. In the following, we focus on the moiré mini-bands featuring a honeycomb lattice[41, 46, 47]. We focus on the regime in which the two sublattices of the effective moiré honeycomb model feature Wannier states localized in different layers, realizing an effectively staggered honeycomb model. The Wannier Hamiltonian produced by the moiré pattern is written as

$$H = t \sum_{\langle ij \rangle s} c_{i,s}^\dagger c_{j,s} + U \sum_i c_{i\uparrow}^\dagger c_{i\uparrow} c_{i\downarrow}^\dagger c_{i\downarrow} + V \sum_{\langle ij \rangle ss'} c_{i,s}^\dagger c_{i,s} c_{j,s'}^\dagger c_{j,s'}, \quad (1)$$

where  $t$  is the first neighbor hopping,  $U$  the on-site Coulomb interaction and  $V$  the first neighbor Coulomb interaction,  $c_{i,s}^\dagger$  and  $c_{j,s'}$  are the usual creation and annihilation fermionic operators for the Wannier moiré orbitals  $i$  and  $j$ . As a reference, the effective value of  $t$  for the twisted dichalcogenide system can be tuned from 1 to 50 meV depending on the twist angle[43, 47–49], and the values of  $U$  and  $V$  range from 5 to 100 meV depending on twist angle and screening effects[49–52]. Long-range interactions run between neighboring moiré Wannier orbitals  $\langle ij \rangle$ . A schematic of the model is shown in Fig. 1b. We will focus on the quarter-filling limit, a regime that can be experimentally reached by electronic gating of the mini-bands.

The interacting model is solved using a self-consistent mean-field procedure including all the Wick contractions, including magnetic symmetry breaking, hopping renormalization, and charge order. In the case of a multiferroic with electric and magnetic orders these order parameters are the electric polarization  $P$  stemming from the staggered nature of the lattice:

$$P = d \left( \sum_s \langle c_{BA,s}^\dagger c_{BA,s} \rangle - \sum_s \langle c_{AB,s}^\dagger c_{AB,s} \rangle \right) \quad (2)$$

where  $d$  is the vertical distance between sublattices that corresponds to the bilayer width, which we will take in natural units  $d = 1$ . The magnetization in the  $z$ -direction on each of the sites  $M_\alpha$ , ( $\alpha = AB, BA$ ) is given by

$$M_\alpha = \sum_s \sigma_z^{ss} c_{\alpha,s}^\dagger c_{\alpha,s} = \langle c_{\alpha,\uparrow}^\dagger c_{\alpha,\uparrow} \rangle - \langle c_{\alpha,\downarrow}^\dagger c_{\alpha,\downarrow} \rangle. \quad (3)$$

and  $M = \sum_\alpha M_\alpha$ . A non-zero value on these order parameters induced by the interactions  $U, V$  indicates the spontaneous emergence of the associated magnetic or charge order. A multiferroic behavior will occur when both order parameters  $P$  and  $M$  are simultaneously different than zero.

## MULTIFERROIC ORDER FROM COMPETING INTERACTIONS

The resulting phase diagram at quarter filling of the interacting Hamiltonian (eq. (1)) for the different order parameters is shown in Fig. 2. Figures 2ab show the phase diagram as a function of the on-site  $U$  and first neighbor

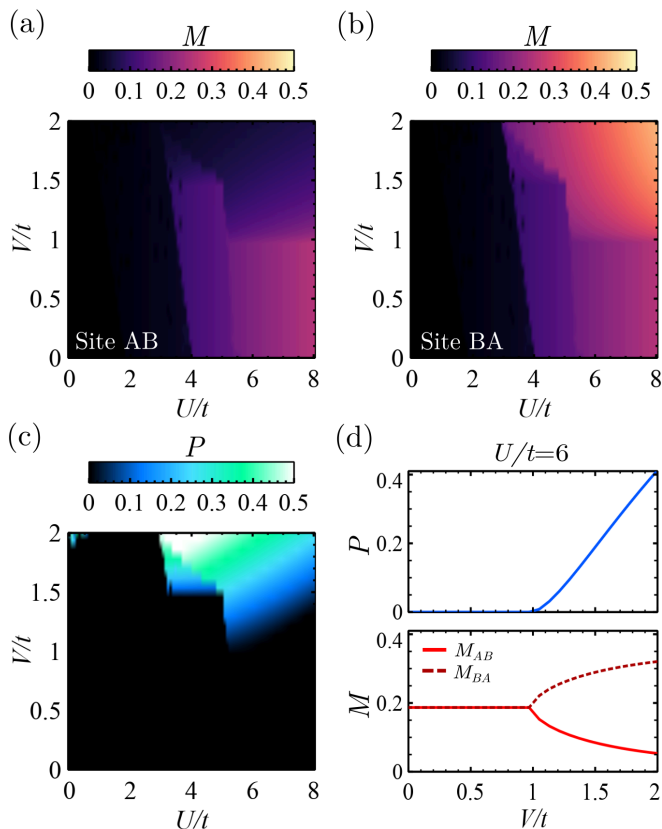


FIG. 2. Emergence of the multiferroic order. (a,b,c) Phase diagrams as a function of the on-site  $U$  and first neighbor  $V$  Coulomb interactions for the different order parameters defined in the text: Magnetization  $M$  on sites AB (a) and BA (b), and electric polarization  $P$  (c). Magnetization is promoted by  $U$  interactions, and  $V$  interactions promote a sublattice imbalance that generates a finite electric polarization. A ferrimagnetic phase and a fully gapped charge density wave coexist in the top-right region of the phase diagram. This multiferroic behavior can be better seen in a cut at  $U/t = 6$ . (d) Order parameters as a function of  $V/t$  for  $U/t = 6$ ,  $P$  ( $M$ ) in the top (bottom) panel. For  $V/t > 1$  both order parameters present a finite value and the magnetization on each site becomes inequivalent.

$V$  Coulomb interactions for the magnetization in each of the sites AB and BA respectively. It can be seen how on-site interactions promote magnetism in the system (right side of the phase diagrams). For  $U/t > 4$  a spontaneous magnetization emerges in both sites of the lattice. Figure 2c shows the phase diagram for the electric polarization. It can be seen that the combination of on-site and first neighbor Coulomb interaction leads to the emergence of an electric polarization  $P$  (top right corner of the phase diagram). The emergence of the electric polarization is a consequence of the spontaneous charge order, promoted by first neighbor Coulomb interactions, between sites AB and BA. In a staggered honeycomb lattice, a staggered charge order produces a net electric polarization in the perpendicular direction, leading to a ferroelectric dipole.

Therefore, the simultaneous emergence of the magnetic and ferroelectric orders constitutes a multiferroic order in the system, like the one depicted in Fig. 1c.

The emergence of the multiferroicity can be rationalized in Fig. 2d. There, a plot of both orders  $P$  and  $M$  as a function of  $V$  is shown fixing  $U/t = 6$ . It can be seen that for  $V/t < 1$  a ferromagnetic order occurs where both sites display the same magnetization and, for the same  $V$  values, no net polarization is present in the system. For  $V/t > 1$  a stagger charge order is promoted as a function of  $V$ , creating a spontaneous electric polarization and leading the ferromagnetic order to a ferrimagnetic one. Associated with the charge order, the magnetization in each of the sites becomes different, a feature that is directly reflecting a magneto-electric coupling. The spin polarized situation and the stagger charge order can be observed in the band structure shown in Fig. 3a. At quarter-filling a gap opens due to Coulomb interactions, promoting a spin polarized situation and the charge gets more localized on the BA site, creating a sublattice imbalance. Consequently, the multiferroic order that emerges from the interplay between  $U$  and  $V$  in the interacting Hamiltonian of eq. (1) is a combination of ferroelectric and ferrimagnetic orders.

A fundamental feature of multiferroic systems that display simultaneously electric and magnetic orders is the magnetoelectric coupling[33]. It refers to the existing coupling between the different order parameters associated with each of the ferroic states. In particular, a strong magnetoelectric coupling allows controlling one of the orders by tuning the other one[35, 53]. Multiferroics whose microscopic mechanism leads to the simultaneous emergence of both orders are known as type-II multiferroics[31, 32]. Their ferroic orders are not independent and therefore a strong magnetoelectric coupling is expected. In the system that we are studying multiferroicity arises due to the combination of competing electronic interactions, leading to the simultaneous emergence of a ferroelectric and a ferrimagnetic order. Therefore, we might expect a strong magnetoelectric coupling in this twisted multiferroic. In order to analyze that, we will include in the interacting Hamiltonian of eq. (1) the effect of an external electric field ( $E$ ) perpendicular to the layers that directly couples to the ferroelectric dipole. This term takes the form

$$H_E = E \sum_s \left[ c_{AB,s}^\dagger c_{AB,s} - c_{BA,s}^\dagger c_{BA,s} \right], \quad (4)$$

which is nothing but a bias difference between Wannier orbitals in the AB and BA due to the staggered nature of the honeycomb lattice.

Figure 3b shows the evolution of the electric polarization  $P$  and magnetization  $M$  on each of the sites as a function of the electric field  $E$ . It can be seen that increasing the electric field increases the electric polariza-

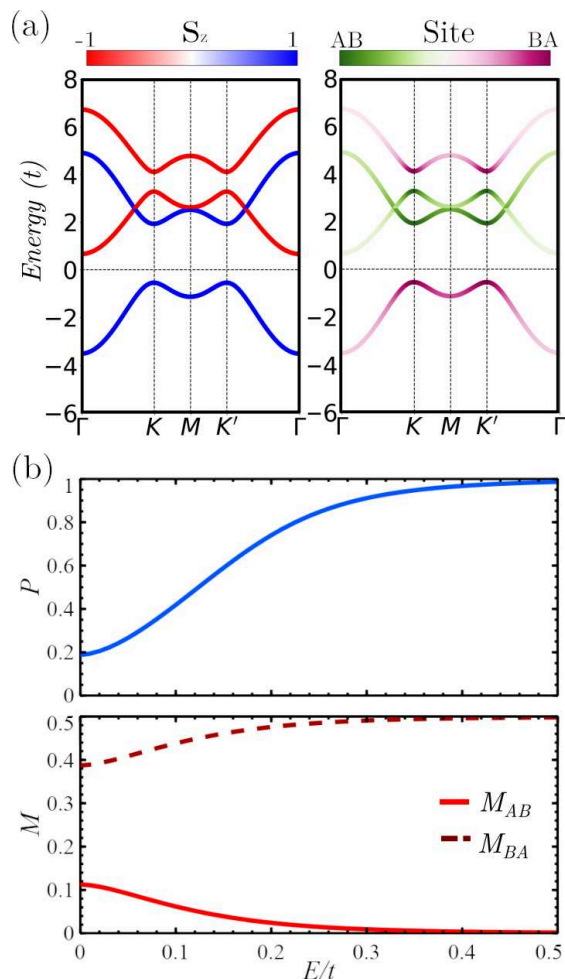


FIG. 3. Calculations in the multiferroic regime at  $U/t = 6$  and  $V/t = 1.5$ . (a) Band structure, the colormaps represent the eigenvalue of the operator:  $s_z$  (sublattice site) in the left (right) panel. A spin polarized and sublattice situation can be identified. (b) Magnetoelectric coupling analysis. Evolution of the order parameters  $P$  (top panel) and  $M$  (bottom panel) as a function of an external electric field in the  $z$ -direction. Due to the strong magnetoelectric coupling, both the electric polarization and the ferrimagnetic order are controlled with the external electric field. The orders saturate at  $E/t = 0.5$ .

tion as expected for a ferroelectric. Moreover, the module of the magnetization on each of the sites gets modified by the electric field, thus providing electric control of the ferrimagnetic order. These results show clear evidence of strong magnetoelectric coupling in the twisted multiferroic. It is worth noting that while the direction of the ferroelectric polarization is locked to the out-of-plane direction, the direction of the magnetization does not have any preferential direction. In the absence of spin-orbit coupling, only the modules of the ferroic order parameters are magnetoelectrically coupled in the interacting Hamiltonian that we are considering.

## TOPOLOGICALLY NON-TRIVIAL MOIRE MULTIFERROIC

So far we have shown that a multiferroic behavior can emerge in the twisted system as a consequence of Coulomb interactions. Another important aspect associated to twisted TMDs is the possible realization of non-trivial topological states[54]. This section will aim to analyze the potential emergence of topological excitations associated with the twisted multiferroic system that we are studying. Transition metal dichalcogenides are well known to show strong spin-orbit coupling effects[55–57], which are known to account for the emergence of topological phase transitions[54]. In particular, the breaking of mirror symmetry in our system triggers the emergence of a Rashba SOC interaction in the low energy effective model[55, 58]. In our twisted system, either the emergence of the out-of-plane electric polarization, or the inclusion of a substrate break mirror symmetry. Furthermore, the use of Janus transition metal dichalcogenides[59–61] would provide a built-in mirror symmetry breaking triggering a large intrinsic Rashba SOC effect[45]. The projection onto the low energy model of the effective Rashba SOC interaction takes the form:

$$H_R = i\lambda_R \sum_{\langle ij \rangle, ss'} \hat{\mathbf{z}} \cdot (\sigma_{s,s'} \times \mathbf{d}_{ij}) c_{i,s}^\dagger c_{j,s'}, \quad (5)$$

where the sum runs over the first neighbors,  $\lambda_R$  controls the strength of the Rashba interaction,  $\mathbf{d}_{ij}$  represents a unit vector pointing from the site  $j$  to  $i$ ,  $\sigma$  are the Pauli matrices and  $\hat{\mathbf{z}}$  is a unit vector along the  $z$ -direction.

We show the interacting electronic structure in Figure 4a, where the effect of the Rashba interaction in the multiferroic regime is observed. At low values of  $\lambda_R$  (left panel), the insulating system has a Chern number  $\mathcal{C} = 0$  and therefore displays a trivial topological character. At high enough values of  $\lambda_R$  (right panel), a band inversion occurs, leading to a non-zero Chern number and turning the multiferroic system into a Chern insulator. This topological transition driven by Rashba spin-orbit coupling can be better analyzed in Fig. 4b. In that plot the interacting Hamiltonian (eq. (1)) is solved including both the electric field term (eq. (4)) and the Rashba SOC interaction (eq. (5)) in the multiferroic regime ( $U/t = 6$  and  $V/t = 1.5$ ). A phase diagram of the topological character (Chern number  $\mathcal{C}$ ) as a function of the electric field  $E$  and the Rashba SOC  $\lambda_R$  is shown in Fig. 4b. The boundary between the orange ( $\mathcal{C} = -1$ ) and blue ( $\mathcal{C} = 0$ ) regions is where the band gap closes leading to a band inversion and consequently to a topological phase transition. Interestingly, in this phase diagram, we can see that the external electric field can cause a topological transition at a given value for the Rashba SOC (see the dashed

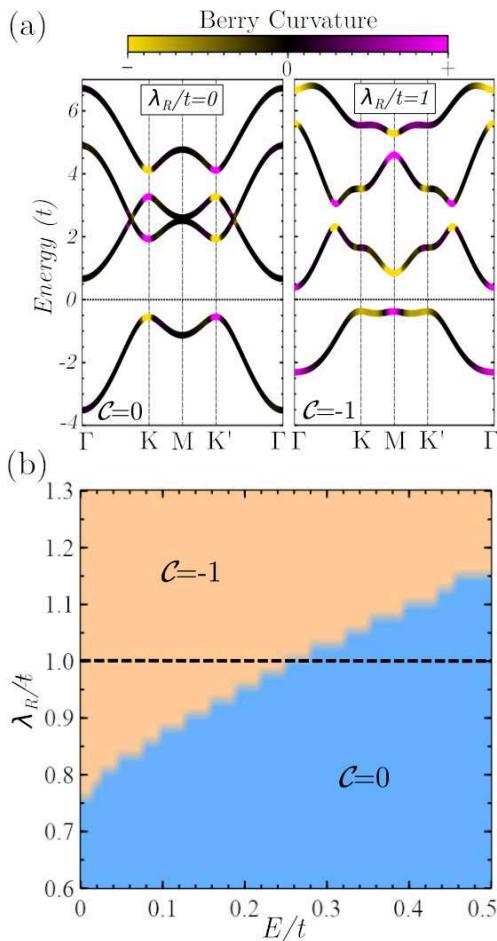


FIG. 4. Topological analysis of the interacting Hamiltonian at  $U/t = 6$  and  $V/t = 1.5$ . (a) Effect of the Rashba spin orbit coupling ( $\lambda_R/t$ ) in the band structure, Berry curvature and Chern number  $\mathcal{C}$ : for  $\lambda_R = 0$ ,  $\mathcal{C} = 0$  (left panel) and for  $\lambda_R = 1.0$ ,  $\mathcal{C} = -1$  (right panel). (c) Phase diagram of the Chern number as a function of  $\lambda_R/t$  and the external electric field bias  $E/t$ . At a given value of  $\lambda_R$  (for instance  $\lambda_R = 1.0$ , dashed line) it is possible to modify the topological character of the system with an electric bias.

line at  $\lambda_R/t = 1$ ). This result shows that it is possible to control the topological character of this system via external electric fields. Therefore, this, together with the multiferroic character of the twisted system, will lead to a magnetoelectric control of diverse topological excitations in the ferroic domain walls of this twisted system as we will address in the next section.

### TOPOLOGICAL MODES IN MULTIFERROIC DOMAINS

In a conventional multiferroic material, different domains are expected to emerge when the sample is cooled at applied electric and magnetic fields. Furthermore, by local application of electric fields, junctions between dif-

ferent multiferroic domains can be engineered. In this section, we address the emergence of topological interface modes in the different domain walls that can occur in the topological multiferroic. In particular, we can encounter purely ferroelectric domains, purely ferrimagnetic domains, and simultaneously ferroelectric and ferrimagnetic domains. The topological character of each of these domains can be controlled by an external electric field as addressed in the previous section. This will allow the manipulation of the emergent interface-topological states. Furthermore, we will show how the underlying modulations induced by a substrate naturally lead to the emergence of topological modes associated to a new supermoire length scale[62–64].

### Tunable topological states in domain walls

Up to this point, we have been based all the analyses on a full selfconsistent solution of the interacting Hamiltonian of eq. (1). Since we will analyze now interfaces between different ferroic domains, in this section we will take a minimal effective mean-field Hamiltonian corresponding to the uniform limit, yet without solving selfconsistently the interface problem. Since the origin of the interface modes is topological, small reconstructions at the interface will not impact the boundary modes. The effective mean-field Hamiltonian takes the form

$$\begin{aligned}
 H_N = & \tilde{t} \sum_{\langle ij \rangle s} c_{i,s}^\dagger c_{j,s} + m \sum_s \left[ c_{AB,s}^\dagger c_{AB,s} - c_{BA,s}^\dagger c_{BA,s} \right] \\
 & + \Delta_Z \sum_{i,s} \sigma_{ss'}^z c_{i,s}^\dagger c_{i,s'} + H_E + H_R,
 \end{aligned} \tag{6}$$

where  $\tilde{t}$  is the moire hopping renormalized by the Coulomb interactions,  $m$  accounts for the interaction-induced charge order accounting for the emergence of the electric polarization, and  $\Delta_Z$  is the interaction induced exchange field associated with the spin polarization in the system. From the microscopic point of view, the three parameters depend on the interactions  $U$  and  $V$ . At quarter-filling values with  $m/t = 0.6$  and  $\Delta_Z/t = 2.0$ , the previous Hamiltonian is analogous to the mean-field result obtained selfconsistently above. In the following we will include the external electric field  $H_E$  (eq. (4)) and Rashba spin-orbit coupling  $H_R$  (eq. (5)) in eq. (6). These terms account for the magnetoelectric coupling and the non-trivial topological character in the effective Hamiltonian.

A schematic of a device showing a minimal interface displaying topological excitations between ferroic domains is shown in Fig. 5a. In a sample with two domains, left (L) and right (R), external electric fields  $E_L$  and  $E_R$  allow controlling the topological character in each of

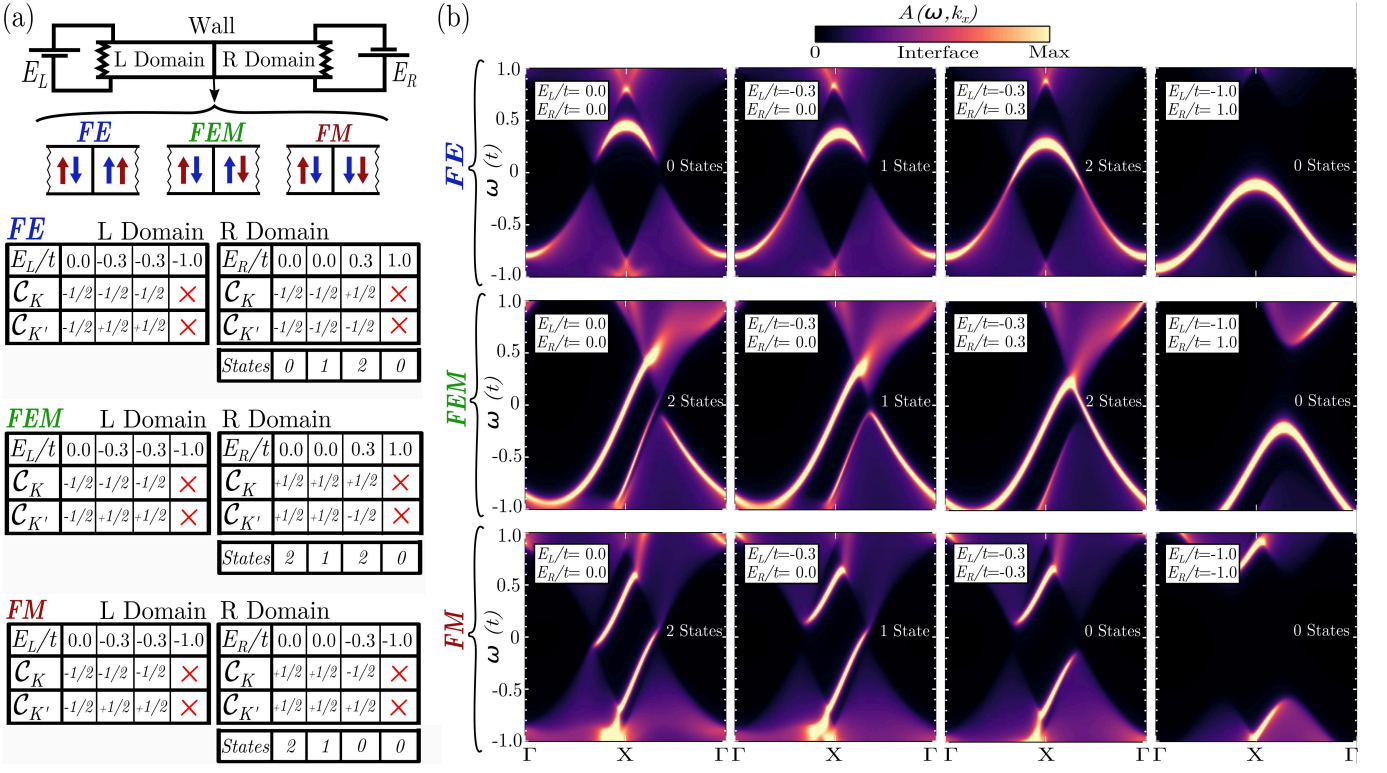


FIG. 5. Magnetoelectric control of topological excitations in the domain walls of a topological multiferroic. (a) Schematic device that allows controlling the topological character of two connected ferroic domains, L (left) and R (right) domains, with external electric fields,  $E_L$  and  $E_R$  respectively. Three different ferroic domain walls can occur:  $FE$  purely ferroelectric,  $FM$  purely ferrimagnetic and  $FEM$  simultaneously ferroelectric and ferrimagnetic. The tables summarize the value of the valley Chern numbers  $C_K$  and  $C_{K'}$  as a function of the external electric fields for each kind of domain wall. The number of emergent interface states is also included. (b) Momentum resolved interface spectral function  $A(\omega, k_x)$  for each of the domain walls  $FE$  (top panels),  $FEM$  (middle panels) and  $FM$  (bottom panels) and for the different  $E_L$  and  $E_R$  values summarized in the tables of panel (a). The calculations were performed with the effective Hamiltonian (eq.(6)) considering  $|m/t| = 0.6$ ,  $|\Delta_Z/t| = 2.0$  and  $\lambda_R/t = 0.8$ .

them. Due to the existence of two valleys  $K$  and  $K'$  in the underlying electronic structure, a valley flux  $C_K$  and  $C_{K'}$  can be defined. Given that the Berry curvature is strongly localized around each valley, the total Chern number becomes  $C = C_K + C_{K'}$ , and the so-called valley Chern number is given by  $C_V = C_K - C_{K'}$ . In the absence of inter-valley scattering, the valley is a good quantum number, each valley becomes independent and the valley Chern number  $C_V$  becomes quantized. Each valley can provide a topological flux of  $\pm 1/2$ , whose sign is determined by the combination of magnetic and electronic symmetry breaking, and act as an independent topological source. Therefore, at the different ferroic domain walls (Fig. 5a) the emergence of an interface state at the  $K$  ( $K'$ ) point is determined by  $C_{K,R} - C_{K,L}$  ( $C_{K',R} - C_{K',L}$ ), i.e., the difference between the corresponding valley Chern numbers of domains R and L. The Chern number difference in each sector can be  $\pm 1$  or 0. A non-zero value implies the emergence of a topological interface state in that valley sector. Therefore, since there are two independent sectors ( $K$  and  $K'$ ), the number of

topological excitations that we can encounter at the interface can be 2, 1, or 0. Moreover, for finite values in the difference between valley Chern numbers ( $\pm 1$ ), the sign at each valley determines the direction of propagation of the interface states. When the total number of interface states is 2, an opposite sign will indicate that both states counter-propagate, while the same sign will indicate co-propagation. Tables summarizing all the possible situations that can occur as a function of the external electric fields for each domain ( $E_L$  and  $E_R$ ) are shown in Fig. 5a. At huge value of the external electric fields ( $E/t = \pm 1.0$  in the tables), valley Chern numbers are no longer good topological numbers due to intervalley mixing, and each domain is simply a trivial multiferroic. Consequently, no interface states will emerge in this limit situation.

In order to demonstrate the emergence of topological interface states for each of the situations summarized in the tables of Fig. 5a, we have computed the momentum resolved interface spectral function  $A(\omega, k_x)$ . This is shown in Fig. 5b for all the different situations. In the case of purely ferroelectric domains ( $FE$  top panels) in-

creasing the value of the external electric fields drives the system from 0, 1, 2 counter-propagating and 0 interface states. In the case of purely ferrimagnetic domains (*FM* bottom panels) increasing the value of the external electric fields drives the system from 2 co-propagating states to 1 state and ultimately 0 interface states at large bias. In the case of simultaneous ferrimagnetic and ferroelectric domains (*FEM* middle panels) increasing the value of the external electric fields drives the system from 2 co-propagating states, 1 state, 2 counter-propagating, and ultimately at large bias 0 interface states. Therefore, these results prove the magnetoelectric control that can be achieved on the topological excitations of this topological multiferroic.

### Topological domains in a supermoire

So far, we have considered that the twisted bilayer dichalcogenide displays a single moire pattern, whose length scale  $L_M$  gives rise to the emergent staggered honeycomb lattice. However, in real moire systems, a substrate is also present (as depicted in Fig. 6a). In particular, the lattice of an underlying substrate, such as boron nitride, gives rise to an additional supermoire pattern between each dichalcogenide[62–64]. When projected on the nearly flat bands of the twisted system, this additional supermoire pattern gives rise to a modulation of the original effective moire superlattice. As sketched in Fig. 6b, from the point of view of the effective low energy model of the moire system, this underlying supermoire pattern gives rise to a modulation in space of the moire model[65, 66]. In the following, and for the sake of concreteness, the unit cell associated with the combination of the moire pattern of the substrate and the twisted dichalcogenide will be denoted as the ultracell and will have an associated lattice parameter  $L_{SM}$  that will be commensurate with the original moire supercell with lattice parameter  $L_M$  (see Fig. 6b).

We now analyze the effect of a substrate on the twisted topological multiferroic. As noted above, a substrate induces a supermoire potential in the twisted system as shown in Fig. 6b. When projected in the Wannier moire orbitals, this modulation gives rise to an electrostatic potential that modulates the staggered Wannier honeycomb lattice that describes the twisted topological multiferroic. As shown in Fig. 6c, we introduce a modulated external field commensurate with a  $30 \times 30$  ultracell, i.e.  $L_{SM} = 30L_M$ , and analyze how the substrate might also lead to the emergence of topological excitations using the effective multiferroic Wannier Hamiltonian (eq. (6)). This modulated potential creates regions with different topological charges,  $C = 0$  on the maximum values of the potential and  $C = -1$  for the minimum values. As a consequence, in the interface between these two topological regions zero energy states appear. In Fig. 6d, the local

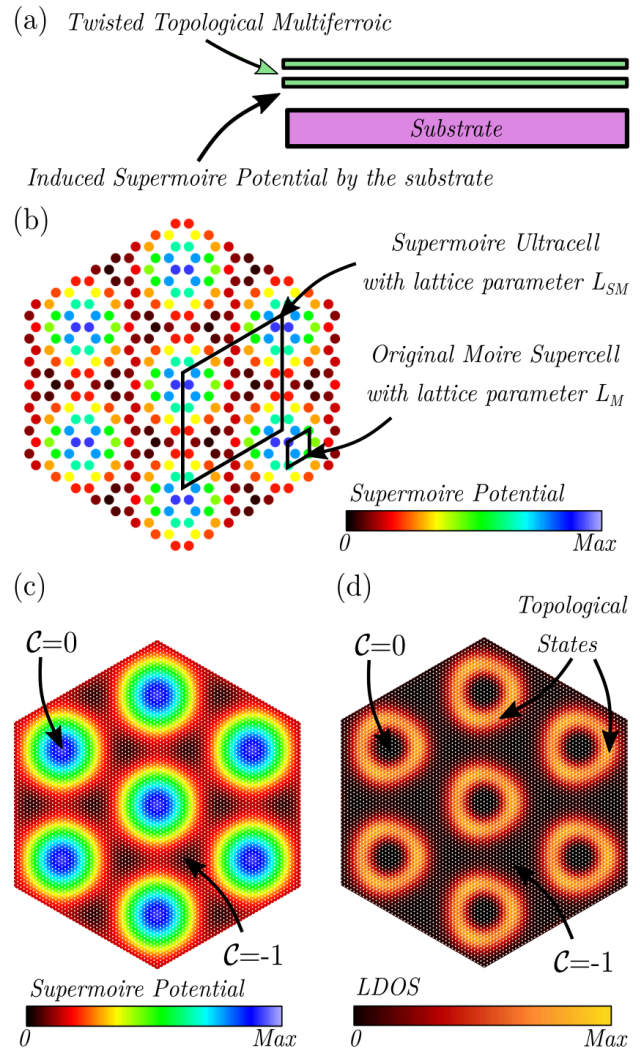


FIG. 6. (a) Effect of a substrate on a twisted topological multiferroic. A supermoire potential is induced in the twisted system by the substrate. (b) Sketch of the supermoire potential on the staggered honeycomb lattice. The external field commensurates with a  $5 \times 5$  ultracell of the staggered honeycomb lattice,  $L_{SM} = 5L_M$ . (c) Supermoire potential of  $L_{SM} = 30L_M$  used in the calculations. The electric potential creates a modulation with different topological-charge regions,  $C = 0$  on the maximum values of the potential and  $C = -1$  for the minimum values. (d) Local density of states (LDOS) at zero energy for the  $L_{SM} = 30L_M$  supermoire potential shown in panel (c). Circular topological states emerge at the boundaries of regions with different topological charge, i.e. inside and outside of the emergent circles.

density of states at zero energy is plotted. We can observe that circular topological states emerge in the topological multiferroic. These zero energy states are commensurate with the modulation created by the substrate. Therefore, the substrate can also be seen as a source of topological excitations for the twisted topological multiferroic that we have studied.

## CONCLUSIONS

To summarize, we have shown how a topological multiferroic order can emerge in twisted transition metal dichalcogenide bilayers. The staggered honeycomb lattice produced by the moire system can be described by an interacting Wannier Hamiltonian with on-site and first neighbor Coulomb interactions. We have shown that, at quarter-filling, on-site interactions lead to a spin polarized system displaying a magnetic order, while first neighbor interactions promote a charge order leading to a spontaneous electric polarization. As a result, the combination of competing repulsive interactions leads to a multiferroic order displaying simultaneously ferroelectric and ferrimagnetic orders. A strong magnetoelectric coupling emerges due to the coupling between charge and spin degrees of freedom promoted by the competing interactions. We further showed that the inclusion of spin-orbit interactions associated to mirror symmetry breaking leads to a topologically non-trivial multiferroic order. We showed that the topological multiferroic displays topological excitations at the different ferroic domain walls, both in the spin and charge sectors. In particular, we have shown that external magnetoelectric control of these topological excitations can be achieved with external electric fields. Finally, by including the impact of an underlying substrate in the moire system, we showed the emergence of topological excitations created by the supermoire on the twisted topological multiferroic. Our findings put forward twisted dichalcogenides as a promising platform to engineer a topological multiferroic order. Finally, our results pave the way to achieve magnetoelectrically-tunable topological excitations, providing a starting point towards the potential use of topological multiferroic modes in quantum technologies.

## ACKNOWLEDGEMENTS

We acknowledge the computational resources provided by the Aalto Science-IT project, and the financial support from the Academy of Finland Projects No. 331342 and No. 336243, and the Jane and Aatos Erkkö Foundation. We thank P. Liljeroth and M. Amini for useful discussions.

---

[1] E. Suárez Morell, J. D. Correa, P. Vargas, M. Pacheco, and Z. Barticevic, “Flat bands in slightly twisted bilayer graphene: Tight-binding calculations,” *Phys. Rev. B* **82**, 121407 (2010).

[2] Yuan Cao, Valla Fatemi, Ahmet Demir, Shiang Fang, Spencer L. Tomarken, Jason Y. Luo, Javier D. Sanchez-Yamagishi, Kenji Watanabe, Takashi Taniguchi, Efthimios Kaxiras, Ray C. Ashoori, and Pablo Jarillo-

Herrero, “Correlated insulator behaviour at half-filling in magic-angle graphene superlattices,” *Nature* **556**, 80–84 (2018).

[3] Yuan Cao, Valla Fatemi, Shiang Fang, Kenji Watanabe, Takashi Taniguchi, Efthimios Kaxiras, and Pablo Jarillo-Herrero, “Unconventional superconductivity in magic-angle graphene superlattices,” *Nature* **556**, 43–50 (2018).

[4] Xiaobo Lu, Petr Stepanov, Wei Yang, Ming Xie, Mohammed Ali Aamir, Ipsita Das, Carles Urgell, Kenji Watanabe, Takashi Taniguchi, Guangyu Zhang, Adrian Bachtold, Allan H. MacDonald, and Dmitri K. Efetov, “Superconductors, orbital magnets and correlated states in magic-angle bilayer graphene,” *Nature* **574**, 653–657 (2019).

[5] Eva Y. Andrei, Dmitri K. Efetov, Pablo Jarillo-Herrero, Allan H. MacDonald, Kin Fai Mak, T. Senthil, Emanuel Tutuc, Ali Yazdani, and Andrea F. Young, “The marvels of moiré materials,” *Nature Reviews Materials* **6**, 201–206 (2021).

[6] Dante M. Kennes, Martin Claassen, Lede Xian, Antoine Georges, Andrew J. Millis, James Hone, Cory R. Dean, D. N. Basov, Abhay N. Pasupathy, and Angel Rubio, “Moiré heterostructures as a condensed-matter quantum simulator,” *Nature Physics* **17**, 155–163 (2021).

[7] Shaowen Chen, Minhao He, Ya-Hui Zhang, Valerie Hsieh, Zaiyao Fei, K. Watanabe, T. Taniguchi, David H. Cobden, Xiaodong Xu, Cory R. Dean, and Matthew Yankowitz, “Electrically tunable correlated and topological states in twisted monolayer–bilayer graphene,” *Nature Physics* **17**, 374–380 (2020).

[8] Cheng Shen, Yanbang Chu, QuanSheng Wu, Na Li, Shuopei Wang, Yanchong Zhao, Jian Tang, Jieying Liu, Jinpeng Tian, Kenji Watanabe, Takashi Taniguchi, Rong Yang, Zi Yang Meng, Dongxia Shi, Oleg V. Yazyev, and Guangyu Zhang, “Correlated states in twisted double bilayer graphene,” *Nature Physics* **16**, 520–525 (2020).

[9] Xiaomeng Liu, Zeyu Hao, Eslam Khalaf, Jong Yeon Lee, Yuval Ronen, Hyobin Yoo, Danial Haei Najafabadi, Kenji Watanabe, Takashi Taniguchi, Ashvin Vishwanath, and Philip Kim, “Tunable spin-polarized correlated states in twisted double bilayer graphene,” *Nature* **583**, 221–225 (2020).

[10] Guorui Chen, Lili Jiang, Shuang Wu, Bosai Lyu, Hongyuan Li, Bheema Lingam Chittari, Kenji Watanabe, Takashi Taniguchi, Zhiwen Shi, Jeil Jung, Yuanbo Zhang, and Feng Wang, “Evidence of a gate-tunable mott insulator in a trilayer graphene moiré superlattice,” *Nature Physics* **15**, 237–241 (2019).

[11] Jeong Min Park, Yuan Cao, Kenji Watanabe, Takashi Taniguchi, and Pablo Jarillo-Herrero, “Tunable strongly coupled superconductivity in magic-angle twisted trilayer graphene,” *Nature* **590**, 249–255 (2021).

[12] M. Serlin, C. L. Tschirhart, H. Polshyn, Y. Zhang, J. Zhu, K. Watanabe, T. Taniguchi, L. Balents, and A. F. Young, “Intrinsic quantized anomalous hall effect in a moiré heterostructure,” *Science* **367**, 900–903 (2020).

[13] Kevin P. Nuckolls, Myungchul Oh, Dillon Wong, Biao Lian, Kenji Watanabe, Takashi Taniguchi, B. Andrei Bernevig, and Ali Yazdani, “Strongly correlated chern insulators in magic-angle twisted bilayer graphene,” *Nature* **588**, 610–615 (2020).

[14] H. Polshyn, J. Zhu, M. A. Kumar, Y. Zhang, F. Yang, C. L. Tschirhart, M. Serlin, K. Watanabe, T. Taniguchi, A. H. MacDonald, and A. F. Young, “Electrical switch-



- ing of magnetic order in an orbital chern insulator,” *Nature* **588**, 66–70 (2020).
- [15] Augusto Ghiotto, En-Min Shih, Giancarlo S. S. G. Pereira, Daniel A. Rhodes, Bumho Kim, Jiawei Zang, Andrew J. Millis, Kenji Watanabe, Takashi Taniguchi, James C. Hone, Lei Wang, Cory R. Dean, and Abhay N. Pasupathy, “Quantum criticality in twisted transition metal dichalcogenides,” *Nature* **597**, 345–349 (2021).
- [16] Tingxin Li, Shengwei Jiang, Bowen Shen, Yang Zhang, Lizhong Li, Zui Tao, Trithep Devakul, Kenji Watanabe, Takashi Taniguchi, Liang Fu, Jie Shan, and Kin Fai Mak, “Quantum anomalous hall effect from intertwined moiré bands,” *Nature* **600**, 641–646 (2021).
- [17] Tingxin Li, Shengwei Jiang, Lizhong Li, Yang Zhang, Kaifei Kang, Jiacheng Zhu, Kenji Watanabe, Takashi Taniguchi, Debanjan Chowdhury, Liang Fu, Jie Shan, and Kin Fai Mak, “Continuous mott transition in semiconductor moiré superlattices,” *Nature* **597**, 350–354 (2021).
- [18] Nai Chao Hu and Allan H. MacDonald, “Competing magnetic states in transition metal dichalcogenide moiré materials,” *Phys. Rev. B* **104**, 214403 (2021).
- [19] Yanhao Tang, Lizhong Li, Tingxin Li, Yang Xu, Song Liu, Katayun Barmak, Kenji Watanabe, Takashi Taniguchi, Allan H. MacDonald, Jie Shan, and Kin Fai Mak, “Simulation of hubbard model physics in WSe<sub>2</sub>/WS<sub>2</sub> moiré superlattices,” *Nature* **579**, 353–358 (2020).
- [20] Lei Wang, En-Min Shih, Augusto Ghiotto, Lede Xian, Daniel A. Rhodes, Cheng Tan, Martin Claassen, Dante M. Kennes, Yusong Bai, Bumho Kim, Kenji Watanabe, Takashi Taniguchi, Xiaoyang Zhu, James Hone, Angel Rubio, Abhay N. Pasupathy, and Cory R. Dean, “Correlated electronic phases in twisted bilayer transition metal dichalcogenides,” *Nature Materials* **19**, 861–866 (2020).
- [21] Emma C. Regan, Danqing Wang, Chenhao Jin, M. Iqbal Bakti Utama, Beini Gao, Xin Wei, Sihan Zhao, Wenyu Zhao, Zuocheng Zhang, Kentaro Yumigeta, Mark Blei, Johan D. Carlström, Kenji Watanabe, Takashi Taniguchi, Sefaattin Tongay, Michael Crommie, Alex Zettl, and Feng Wang, “Mott and generalized wigner crystal states in WSe<sub>2</sub>/WS<sub>2</sub> moiré superlattices,” *Nature* **579**, 359–363 (2020).
- [22] Chenhao Jin, Zui Tao, Tingxin Li, Yang Xu, Yanhao Tang, Jiacheng Zhu, Song Liu, Kenji Watanabe, Takashi Taniguchi, James C. Hone, Liang Fu, Jie Shan, and Kin Fai Mak, “Stripe phases in WSe<sub>2</sub>/WS<sub>2</sub> moiré superlattices,” *Nature Materials* **20**, 940–944 (2021).
- [23] Xiong Huang, Tianmeng Wang, Shengnan Miao, Chong Wang, Zhipeng Li, Zhen Lian, Takashi Taniguchi, Kenji Watanabe, Satoshi Okamoto, Di Xiao, Su-Fei Shi, and Yong-Tao Cui, “Correlated insulating states at fractional fillings of the WS<sub>2</sub>/WSe<sub>2</sub> moiré lattice,” *Nature Physics* **17**, 715–719 (2021).
- [24] Miguel M. Ugeda, Aaron J. Bradley, Yi Zhang, Seita Onishi, Yi Chen, Wei Ruan, Claudia Ojeda-Aristizabal, Hyejin Ryu, Mark T. Edmonds, Hsin-Zon Tsai, Alexander Riss, Sung-Kwan Mo, Dunghai Lee, Alex Zettl, Zahid Hussain, Zhi-Xun Shen, and Michael F. Crommie, “Characterization of collective ground states in single-layer NbSe<sub>2</sub>,” *Nature Physics* **12**, 92–97 (2015).
- [25] Sajedeh Manzeli, Dmitry Ovchinnikov, Diego Pasquier, Oleg V. Yazyev, and Andras Kis, “2d transition metal dichalcogenides,” *Nature Reviews Materials* **2** (2017), 10.1038/natrevmats.2017.33.
- [26] K. Kośmider and J. Fernández-Rossier, “Electronic properties of the mos<sub>2</sub>-ws<sub>2</sub> heterojunction,” *Phys. Rev. B* **87**, 075451 (2013).
- [27] Xiaodong Xu, Wang Yao, Di Xiao, and Tony F. Heinz, “Spin and pseudospins in layered transition metal dichalcogenides,” *Nature Physics* **10**, 343–350 (2014).
- [28] Pasqual Rivera, Kyle L. Seyler, Hongyi Yu, John R. Schaibley, Jiaqiang Yan, David G. Mandrus, Wang Yao, and Xiaodong Xu, “Valley-polarized exciton dynamics in a 2d semiconductor heterostructure,” *Science* **351**, 688–691 (2016).
- [29] Yang Xu, Kaifei Kang, Kenji Watanabe, Takashi Taniguchi, Kin Fai Mak, and Jie Shan, “Tunable bilayer hubbard model physics in twisted wse<sub>2</sub>,” (2022).
- [30] Nicola A. Hill, “Why are there so few magnetic ferroelectrics?” *The Journal of Physical Chemistry B* **104**, 6694–6709 (2000).
- [31] N. A. Spaldin and R. Ramesh, “Advances in magnetoelectric multiferroics,” *Nature Materials* **18**, 203–212 (2019).
- [32] Manfred Fiebig, Thomas Lottermoser, Dennis Meier, and Morgan Trassin, “The evolution of multiferroics,” *Nature Reviews Materials* **1** (2016), 10.1038/natrevmats.2016.46.
- [33] Manfred Fiebig, “Revival of the magnetoelectric effect,” *Journal of Physics D: Applied Physics* **38**, R123–R152 (2005).
- [34] Ce-Wen Nan, M. I. Bichurin, Shuxiang Dong, D. Viehland, and G. Srinivasan, “Multiferroic magnetoelectric composites: Historical perspective, status, and future directions,” *Journal of Applied Physics* **103**, 031101 (2008).
- [35] N. Hur, S. Park, P. A. Sharma, J. S. Ahn, S. Guha, and S.-W. Cheong, “Electric polarization reversal and memory in a multiferroic material induced by magnetic fields,” *Nature* **429**, 392–395 (2004).
- [36] Martin Gajek, Manuel Bibes, Stéphane Fusil, Karim Bouzehouane, Josep Fontcuberta, Agnès Barthélémy, and Albert Fert, “Tunnel junctions with multiferroic barriers,” *Nature Materials* **6**, 296–302 (2007).
- [37] Hwiin Ju, Youjin Lee, Kwang-Tak Kim, In Hyeok Choi, Chang Jae Roh, Suhan Son, Pyeongjae Park, Jae Ha Kim, Taek Sun Jung, Jae Hoon Kim, Kee Hoon Kim, Je-Geun Park, and Jong Seok Lee, “Possible persistence of multiferroic order down to bilayer limit of van der waals material NiI<sub>2</sub>,” *Nano Letters* **21**, 5126–5132 (2021).
- [38] Qian Song, Connor A. Occhialini, Emre Ergeçen, Batyr Ilyas, Danila Amoroso, Paolo Barone, Jesse Kapeghian, Kenji Watanabe, Takashi Taniguchi, Antia S. Botana, Silvia Picozzi, Nuh Gedik, and Riccardo Comin, “Evidence for a single-layer van der waals multiferroic,” *Nature* **602**, 601–605 (2022).
- [39] Adolfo O Fumega and J L Lado, “Microscopic origin of multiferroic order in monolayer NiI<sub>2</sub>,” *2D Materials* **9**, 025010 (2022).
- [40] Note that including the effect of the chalcogen atoms in the twisted system will include an inequivalence between AB and BA sites that will be effectively translated into a small sublattice imbalance in the staggered honeycomb model.
- [41] Yang Zhang, Tongtong Liu, and Liang Fu, “Electronic structures, charge transfer, and charge order in twisted transition metal dichalcogenide bilayers,” *Phys. Rev. B*

- 103**, 155142 (2021).
- [42] Zhen Zhan, Yipei Zhang, Pengfei Lv, Hongxia Zhong, Guodong Yu, Francisco Guinea, José Ángel Silva-Guillén, and Shengjun Yuan, “Tunability of multiple ultraflat bands and effect of spin-orbit coupling in twisted bilayer transition metal dichalcogenides,” *Phys. Rev. B* **102**, 241106 (2020).
- [43] Yipei Zhang, Zhen Zhan, Francisco Guinea, Jose Ángel Silva-Guillén, and Shengjun Yuan, “Tuning band gaps in twisted bilayer  $\text{MoS}_2$ ,” *Phys. Rev. B* **102**, 235418 (2020).
- [44] Somepalli Venkateswarlu, Andreas Honecker, and Guy Trambly de Laissardière, “Electronic localization in twisted bilayer  $\text{MoS}_2$  with small rotation angle,” *Phys. Rev. B* **102**, 081103 (2020).
- [45] D Soriano and J L Lado, “Spin-orbit correlations and exchange-bias control in twisted janus dichalcogenide multilayers,” *New Journal of Physics* **23**, 073038 (2021).
- [46] Lede Xian, Martin Claassen, Dominik Kiese, Michael M. Scherer, Simon Trebst, Dante M. Kennes, and Angel Rubio, “Realization of nearly dispersionless bands with strong orbital anisotropy from destructive interference in twisted bilayer  $\text{MoS}_2$ ,” *Nature Communications* **12** (2021), 10.1038/s41467-021-25922-8.
- [47] Mattia Angeli and Allan H. MacDonald, “ $\gamma$  valley transition metal dichalcogenide moiré bands,” *Proceedings of the National Academy of Sciences* **118** (2021), 10.1073/pnas.2021826118.
- [48] Mit H. Naik and Manish Jain, “Ultraflatbands and shear solitons in moiré patterns of twisted bilayer transition metal dichalcogenides,” *Phys. Rev. Lett.* **121**, 266401 (2018).
- [49] Fengcheng Wu, Timothy Lovorn, Emanuel Tutuc, and A. H. MacDonald, “Hubbard model physics in transition metal dichalcogenide moiré bands,” *Phys. Rev. Lett.* **121**, 026402 (2018).
- [50] Tommaso Cea, Niels R. Walet, and Francisco Guinea, “Electronic band structure and pinning of fermi energy to van hove singularities in twisted bilayer graphene: A self-consistent approach,” *Phys. Rev. B* **100**, 205113 (2019).
- [51] J. M. Pizarro, M. Rösner, R. Thomale, R. Valentí, and T. O. Wehling, “Internal screening and dielectric engineering in magic-angle twisted bilayer graphene,” *Phys. Rev. B* **100**, 161102 (2019).
- [52] Xiaoxue Liu, Zhi Wang, K. Watanabe, T. Taniguchi, Oskar Vafek, and J. I. A. Li, “Tuning electron correlation in magic-angle twisted bilayer graphene using coulomb screening,” *Science* **371**, 1261–1265 (2021).
- [53] T. Kimura, T. Goto, H. Shintani, K. Ishizaka, T. Arima, and Y. Tokura, “Magnetic control of ferroelectric polarization,” *Nature* **426**, 55–58 (2003).
- [54] Fengcheng Wu, Timothy Lovorn, Emanuel Tutuc, Ivar Martin, and A. H. MacDonald, “Topological insulators in twisted transition metal dichalcogenide homobilayers,” *Phys. Rev. Lett.* **122**, 086402 (2019).
- [55] Andor Kormányos, Viktor Zólyomi, Neil D. Drummond, and Guido Burkard, “Spin-orbit coupling, quantum dots, and qubits in monolayer transition metal dichalcogenides,” *Phys. Rev. X* **4**, 011034 (2014).
- [56] K. Kośmider, J. W. González, and J. Fernández-Rossier, “Large spin splitting in the conduction band of transition metal dichalcogenide monolayers,” *Phys. Rev. B* **88**, 245436 (2013).
- [57] Z. Y. Zhu, Y. C. Cheng, and U. Schwingenschlögl, “Giant spin-orbit-induced spin splitting in two-dimensional transition-metal dichalcogenide semiconductors,” *Phys. Rev. B* **84**, 153402 (2011).
- [58] Yu A Bychkov and E I Rashba, “Oscillatory effects and the magnetic susceptibility of carriers in inversion layers,” *Journal of Physics C: Solid State Physics* **17**, 6039–6045 (1984).
- [59] Ang-Yu Lu, Hanyu Zhu, Jun Xiao, Chih-Piao Chuu, Yimo Han, Ming-Hui Chiu, Chia-Chin Cheng, Chih-Wen Yang, Kung-Hwa Wei, Yiming Yang, Yuan Wang, Dimosthenis Sokaras, Dennis Nordlund, Peidong Yang, David A. Muller, Mei-Yin Chou, Xiang Zhang, and Lain-Jong Li, “Janus monolayers of transition metal dichalcogenides,” *Nature Nanotechnology* **12**, 744–749 (2017).
- [60] Jing Zhang, Shuai Jia, Iskandar Kholmanov, Liang Dong, Dequan Er, Weibing Chen, Hua Guo, Zehua Jin, Vivek B. Shenoy, Li Shi, and Jun Lou, “Janus monolayer transition-metal dichalcogenides,” *ACS Nano* **11**, 8192–8198 (2017).
- [61] Liang Dong, Jun Lou, and Vivek B. Shenoy, “Large in-plane and vertical piezoelectricity in janus transition metal dichalcogenides,” *ACS Nano* **11**, 8242–8248 (2017).
- [62] Miša Anđelković, Slaviša P. Milovanović, Lucian Covaci, and François M. Peeters, “Double moiré with a twist: Supermoiré in encapsulated graphene,” *Nano Letters* **20**, 979–988 (2020).
- [63] Zihao Wang, Yi Bo Wang, J. Yin, E. Tóvári, Y. Yang, L. Lin, M. Holwill, J. Birkbeck, D. J. Perello, Shuigang Xu, J. Zultak, R. V. Gorbachev, A. V. Kretinin, T. Taniguchi, K. Watanabe, S. V. Morozov, M. Anđelković, S. P. Milovanović, L. Covaci, F. M. Peeters, A. Mishchenko, A. K. Geim, K. S. Novoselov, Vladimir I. Fal’ko, Angelika Knothe, and C. R. Woods, “Composite super-moiré lattices in double-aligned graphene heterostructures,” *Science Advances* **5** (2019), 10.1126/sciadv.aay8897.
- [64] N Leconte and J Jung, “Commensurate and incommensurate double moire interference in graphene encapsulated by hexagonal boron nitride,” *2D Materials* **7**, 031005 (2020).
- [65] Ziyang Zhu, Paul Cazeaux, Mitchell Luskin, and Efthimios Kaxiras, “Modeling mechanical relaxation in incommensurate trilayer van der waals heterostructures,” *Phys. Rev. B* **101**, 224107 (2020).
- [66] Simon Turkel, Joshua Swann, Ziyang Zhu, Maine Christos, K. Watanabe, T. Taniguchi, Subir Sachdev, Mathias S. Scheurer, Efthimios Kaxiras, Cory R. Dean, and Abhay N. Pasupathy, “Twistons in a Sea of Magic,” arXiv e-prints, arXiv:2109.12631 (2021), arXiv:2109.12631 [cond-mat.str-el].